Composite Structures 107 (2014) 246–259

Contents lists available at ScienceDirect

Composite Structures

journal homepage: www.elsevier.com/locate/compstruct

Hierarchical optimization of laminated fiber reinforced composites

Rafael T.L. Ferreira [a,b,*], Helder C. Rodrigues [a], José M. Guedes [a], José A. Hernandes [b]

[a] IDMEC/IST, Instituto Superior Técnico, Av. Rovisco Pais, 1, 1049-001 Lisbon, Portugal
[b] ITA, Instituto Tecnológico de Aeronáutica, Pça. Mal. Eduardo Gomes, 50, 12228-900 São José dos Campos, SP, Brazil

ARTICLE INFO

Article history:
Available online 6 August 2013

Keywords:
Hierarchical optimization
Laminated composites
Shape of reinforcement fibers

ABSTRACT

The aim of this work is to perform hierarchical optimization in laminated composite structures, considering simultaneously macroscopic and microscopic levels in the design of structure and material. The macroscopic level takes into account orientations and fiber volume fractions of unidirectional composite layers. The microscopic level considers the cross-sectional size and shape of the reinforcement fibers, assuming them elliptical. Both levels are coupled by a resource constraint and exchange derivatives in a mathematically consistent manner.

The objective is to minimize compliance under a total fiber volume fraction constraint. The variation of the fibers' size and shape is considered by response surfaces for constitutive parameters of a reinforced lamina. Such surfaces are built from data evaluated by asymptotic homogenization techniques. The plies orientations are chosen using the Discrete Material Optimization (DMO) approach.

Results in laminated plates show the influence of the reinforcement fibers' shape and volume fraction in their global behavior. The optimal microstructures obtained vary with the loading conditions considered. It is shown that the present optimization procedure permits to increase structural stiffness when material microstructural characteristics are considered. Moreover, an assessment of layers' microstructural stresses is carried out in order to evaluate the fibers' shape influence on stress concentrations.

1. Introduction

The employment of laminated composites in many manufactured products, from tennis rackets to aerospace components, is a reality nowadays. In highly engineered applications, good designs have well explored the characteristic of high stiffness to mass ratio of such materials. For a fixed overall thickness, the resultant mechanical properties of composite laminates may vary a lot with the number of layers, reinforcement fibers' directions and the stacking sequence of layers. Therefore, for a certain application, a common practice is to look for an appropriate (or preferably the best) lay-up for a component, which depends on its mechanical requirements. Numerical optimization techniques were proven to be appropriate tools for this task, as can be noticed from the extensive literature on laminated composites optimization. A few examples of these developments are described in Refs. [1–4].

Besides the stacking sequence characteristics, this paper has the aim of investigating by optimization the influence of other parameters in the global behavior of laminated components, namely related to microstructural details of the plies forming it. These plies are in general (but not exclusively) made by a resin matrix reinforced in one direction by higher strength fibers, and are mostly treated in an analysis/optimization environment as an orthotropic material whose equivalent mechanical properties are fixed and determined by appropriate testing techniques. However, the objective here is to consider such mechanical properties as variable quantities, in terms of the fiber volume fraction and the cross-sectional shape of the fibers used in stiffening the weaker matrix. Here, these cross-sections are assumed elliptical and their dimensions are taken as design variables in an appropriate optimization problem, which is conceived as a compliance minimization subjected to a resource constraint on the admissible total fiber volume fraction. Variables related to the choice of ply orientation are also considered.

As this problem deals with optimization of mechanical characteristics at both the macro (global) and micro (local) structural levels of the composite structure of interest, an approach based on the hierarchical topology optimization model presented in [5] is here employed. In topology optimization problems, a common practice is to employ the SIMP power law to interpolate material properties in terms of an artificial density design variable [6], in order to define material and void distribution over a structure. In hierarchical topology optimization, this interpolation is substituted by a series of other topology optimization problems whose goal is to define the material microstructure. Therefore, it has the aim of designing the material distribution layout of a structure in two distinct

* Corresponding author. Address: DCTA/ITA/IEM, Brazil. Tel.: +55 12 3947 6976; fax: +55 12 3947 5967.
E-mail addresses: rthiago@ita.br (R.T.L. Ferreira), hcr@ist.utl.pt (H.C. Rodrigues).

0263-8223/$ - see front matter © 2013 Elsevier Ltd. All rights reserved.
http://dx.doi.org/10.1016/j.compstruct.2013.07.051

levels: one macromechanical and the other micromechanical, which is done in a simultaneous and integrated way. Such levels can be also identified as global or structural and local or material, respectively. In the first level, design in terms of material distribution on the general layout of the structure is taken into account. In the second level, the design of constitutive properties is treated in terms of defining the distribution of material (and/or void) phases in representative cells of microstructure over the macro-level. The equivalent properties of such microstructures are calculated by asymptotic homogenization techniques [7] and taken into account at the global level.

This multi-level approach has been the focus of research over the recent years, with applications to 3D structures [8], biomechanical models of bone remodeling [9], linear cellular materials [10], fluid–structure interaction problems [11] and nonlinear structures [12], for example. With the advances in new fabrication technologies able to create geometrically intricate products like rapid prototyping, the tendency of this field is to be even more explored in the future, when the designed microstructural details can be reproduced in manufactured components.

The hierarchical optimization has also been applied to layered composites in a recent work [13], where the goal was to define optimal matrix/fiber distribution in the plies' microstructure and also to find fiber volume fraction and reinforcement fiber orientation in such plies, for minimal compliance. In the macro-level, each layer was treated as a group of tridimensional finite elements and representative cells of microstructure had their topology defined in each of the laminae of the composite, in a particularization of the methodology presented in [8]. The results presented were interesting to visualize possible gains in terms of microstructure topology design in fiber reinforced composites, but they were not of promptly applicability in manufacturing.

Based on this insight, the idea here is to treat the microstructure of the composites in a more restrictive way, based on reinforcement fiber shapes that may be commonly produced. Moreover, the composites are treated by plate/shell models, where the modeling of constitutive characteristics classically involves the calculation of equivalent stiffness properties for laminates, by means of appropriate integrals through the thickness of the stacking sequence [14]. The individual laminae properties are those considered variable and this is taken into account by representing such properties by appropriate response surfaces [15], in terms of the dimensions of the elliptical cross-section assumed for the fibers. They consist of third order polynomials which are fitted upon data obtained by asymptotic homogenization applied over a representative microstructure cell counting with the arrangement of the fiber with predefined shape plus the matrix. Function values and derivative information are employed in the fittings [16], in order to enhance the quality of the approximations.

With the goal of also performing optimization in terms of ply orientations, the recent Discrete Material Optimization (DMO) parametrization is employed [17]. It basically consists on the interpolation of candidate materials by proper weighting functions of dedicated design variables. To select the candidate materials among a predefined set of options, such weight functions are defined by optimization.

Thus, the hierarchical approach followed here considers in the macro-level design for fiber volume fractions and orientations over the layers and, in the micro-level, design for fiber cross-sectional dimensions. Sequential Approximate Optimization (SAO) techniques [18,19] are used to solve both the macro/micro-problems. The results in laminated plates show clearly the influence of the fiber shape in the final properties of the laminate and that enhanced structures can be obtained if microstructural details are considered in the optimization. The response surfaces developed also highlight this aspect and help to understand the role of the fiber cross-section shape in the problem.

2. Micromechanical modeling

Fig. 1 shows a schematic representation of the fiber/matrix arrangement of a typical unidirectionally reinforced lamina used in laminated composites, which are made (roughly speaking) from stacking and curing together several of these lamina in different orientations. It is possible to see several fibers reinforcing the matrix in the direction 1 and whose distribution is considered periodic over the matrix domain. In the actual material, such distribution is of course not so well organized but has indeed a strong periodic trend, as can be seen for example from the laminated composites micrographs in [20], which highlights a representative unit cell of the material microstructure, where a small piece of fiber is surrounded by matrix.

Usually, reinforcement fibers in unidirectional composites have circular cross-section. However, in practice, some possible variations on this shape are also reported, which are drawn in the initial stages of the manufacturing process of the fibers. For carbon fibers, several cross-sections may be obtained [21], including elliptical and triangular-like ones [22], for example. For glass fibers, diverse cross-sections shapes are also reported, like oval, peanut-like [23] and triangular [24]. Here, the shape of the fibers cross-section is assumed as elliptical, whose semi-axes are given by the a and b parameters in Fig. 1. This unit cell is considered to appear repeatedly in the composite, many times over the 1, 2 and 3 directions.

Under the assumption of periodicity, asymptotic homogenization [7] may be employed to determine equivalent properties of the composite material unit cell. Such homogenized properties are given by an integral over the volume Y of the cell:

$$E^H_{ijkm} = \frac{1}{|Y|}\int_Y \left(E_{ijkm} - E_{ijrs}\frac{\partial \chi^{km}_r}{\partial y_s}\right) dY \tag{1}$$

The χ^{km}_r are displacement test fields over the unit cell that respect periodicity conditions and are obtained from the following problem in the micro-level:

$$\int_Y E_{ijrs}\frac{\partial \chi^{km}_r}{\partial y_s}\frac{\partial v_i}{\partial y_j} dY = \int_Y E_{ijkm}\frac{\partial v_i}{\partial y_j} dY \tag{2}$$

In this equation the v_i are admissible displacement test functions. This problem comes from the assumption that a laminated composite structure under applied external forces has its global displacements represented by a superposition of displacement functions of slow (in the macro-scale) and rapid (in the micro-scale) variation. The problem for the χ^{km}_r can be solved by the finite element method, discretizing the domain of the unit cell shown. By varying the parameters a and b in the assumed cross-section of the reinforcement fiber, several homogenization problems can be solved to obtain the resulting constitutive properties of the material, which carry the influence of the fiber shape. In this case, due to symmetries in the unit cell, the expected homogenized material E^H_{ijkm} is orthotropic.

Here, the methodology used for obtaining such lamina homogenized constants is based in the software PREMAT [7], which is employed to treat the problem of the unit cell in Fig. 1 by a 3D finite elements approach. It is important to highlight that the procedure of using material homogenized constants obtained from a 3D elasticity problem to represent the constitutive parameters of a lamina in a plate/shell (2D) problem is valid, since it is considered that the microstructure unit cell repeats itself several times over the lamina thickness direction 3, as it is true for unidirectional fiber composites. If this was not the case, as in plain-weave textile composites for example, a proper asymptotic analysis would be recommended

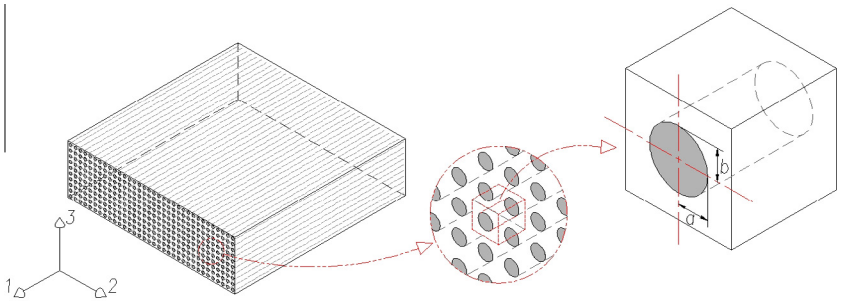

Fig. 1. Scheme for the fiber/matrix arrangement in an unidirectionally reinforced lamina and unit cell of its microstructure.

[25]. Moreover, in [26] it is reported that a periodic homogenization procedure like the one here taken provides a good estimation of material properties of an unidirectional composite in comparison to experimental data.

3. Response surfaces of lamina constitutive parameters

Surrogate models [15] are usually employed in engineering to represent complicated computer experiments over a design space, substituting such experiments by a functional relation of predefined design parameters, that may be used within certain restrictions, depending on how accurate it can be made. They can be employed in highlighting design trends and also in optimization purposes. If the computer experiments have a huge cost, like in many finite element and CFD analyses, such models become useful decision tools [27].

Building a surrogate model involves basically sampling the design space by evaluating a certain quantity in chosen design points, and then fitting these data into a basis of shape functions. Moreover, the generated model is checked in order to assess its quality and may be updated to meet desired fitness requirements. Here, the objective is to represent adequately the constitutive parameters of the composite lamina in Fig. 1 by functions of the fiber shape variables a, b. Namely, the constitutive parameters approximated are the usually designated Q_{ij} of an orthotropic lamina in plane stress, plus the shearing stiffnesses related to out-of-plane shearing, useful in the Reissner–Mindlin plate theory [14]. They are shown in the following equations, also in terms of material engineering constants:

$$\begin{Bmatrix}\sigma_{11}\\ \sigma_{22}\\ \tau_{12}\end{Bmatrix}=\begin{bmatrix}Q_{11} & Q_{12} & 0\\ Q_{12} & Q_{22} & 0\\ 0 & 0 & Q_{66}\end{bmatrix}\begin{Bmatrix}\epsilon_{11}\\ \epsilon_{22}\\ \gamma_{12}\end{Bmatrix}\quad\begin{Bmatrix}\tau_{23}\\ \tau_{13}\end{Bmatrix}=\begin{bmatrix}Q_{44} & 0\\ 0 & Q_{55}\end{bmatrix}\begin{Bmatrix}\gamma_{23}\\ \gamma_{13}\end{Bmatrix} \tag{3}$$

$$Q_{11}=\frac{E_1}{1-\nu_{12}\nu_{21}}\quad Q_{12}=\nu_{21}Q_{11}\quad Q_{22}=\frac{E_2}{1-\nu_{12}\nu_{21}}$$
$$Q_{44}=G_{23}\quad Q_{55}=G_{13}\quad Q_{66}=G_{12} \tag{4}$$

Within this goal, it is employed one of the most common surrogate models: a response surface based in polynomial regression. Namely, a complete cubic polynomial in the a, b parameters is chosen, based on several previous tests where the quantities being approximated showed up to have a smooth variation inside the desired design domain. Besides rendering good material properties approximation, these surrogate models must also provide well approximate derivatives of these properties in terms of the a, b, since the intent is to use them in gradient-based optimization. Therefore, derivative information is used together with function value evaluations in the polynomial fittings, in order to enhance its approximating capabilities. The fitting method is the Iterative Weighted Least Squares (IWLS) [16] that consists in a weighted least squares method with weighting based on an estimative of the fitting errors covariance [28].

The design space sampling is made by latin hypercubes [29], which cover every portion of the ranges of the design variables, using a random generation. However, some latin hypercubes may not fill adequately the design space with sampling points, ending up with some design domain areas not so well covered. Thus, one of its variations is used, the so-called Improved Distributed Hypercube Sampling (IHS) [30], which tries to improve the samples distribution over the design space by proposing hypercubes with the points as much spread out as possible. The response surfaces checking is made upon the following usual accuracy measures: the R^2, the average relative error (*ARE*) and the maximum relative error (*MRE*), in a similar fashion as in [31].

Some of the results obtained using the described methodology are depicted in Figs. 2 and 3, where fittings for the Q_{11} and Q_{66} stiffnesses in Eq. (3) are shown. The design space defined for the a, b variables is given by the intervals $[0.15,0.40]\times[0.15,0.40]$ in terms of relative dimensions, considering the microstructure representative cell in Fig. 1 as an unitary cube. This domain englobes cross-sectional shapes of the reinforcement fiber varying from circular to elliptical. It was sampled by 100 points defined by the IHS method, where homogenized properties and their derivatives were evaluated. Such derivatives were obtained by central finite differences, perturbing the homogenization results. The properties used for fiber and matrix were respectively $E_f = 73$ GPa, $\nu_f = 0.22$ and $E_m = 3.45$ GPa, $\nu_m = 0.35$ [13], typical of glass fiber and epoxi resin matrix, taking both as isotropic.

Fig. 2 shows two plots for the response surface found for Q_{11}. The one on the left side shows a 3D representation of the polynomial fitted in terms of a, b. The graph on the right side shows the same surface but in lines of constant values of volume fraction ρ occupied by the fiber, in terms of the fiber cross-sectional aspect ratio a/b. As the a, b dimensions are defined over an unitary cubic microstructure cell, the volume fraction can be interpreted as the cross sectional area of the fiber or $\rho = \pi ab$. Therefore, looking to the variation of Q_{11} with a/b for the several ρ, these results show that the material constant has no influence of the aspect ratio a/b, since the property is (as expected) constant with it, and varies only due to changes in the volume fraction ρ. In the other hand, from the same plots for Q_{66} shown in Fig. 3, it can be seen that this property has a strong influence of the fiber shape by noticing a big variation on it with the a/b ratio for constant values of ρ, where this stiffness increase with a/b. The response surfaces obtained for other properties in Eq. (3) (Q_{12}, Q_{22}, Q_{44} and Q_{55}) also highlighted some variation of constitutive characteristics with a/b. However, in the results to be shown, the most significative is the variation in Q_{66} followed by the variations in Q_{12} and Q_{22}, which are similar to the Q_{66} variation in terms of having the highest stiffness values at the highest values of the a/b ratio.

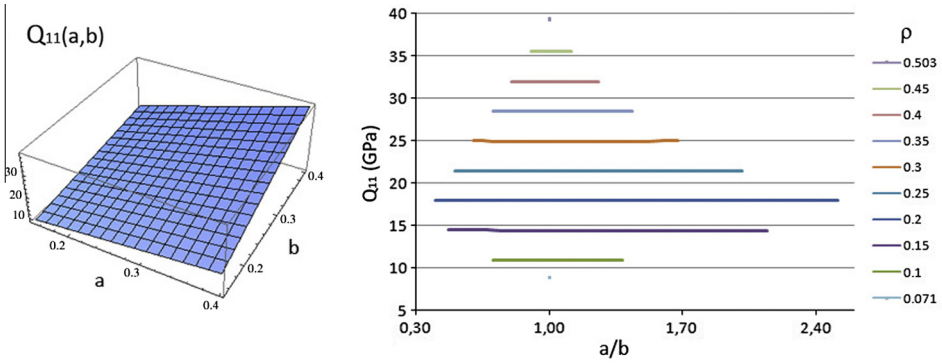

Fig. 2. Plots for the response surface developed for Q_{11}.

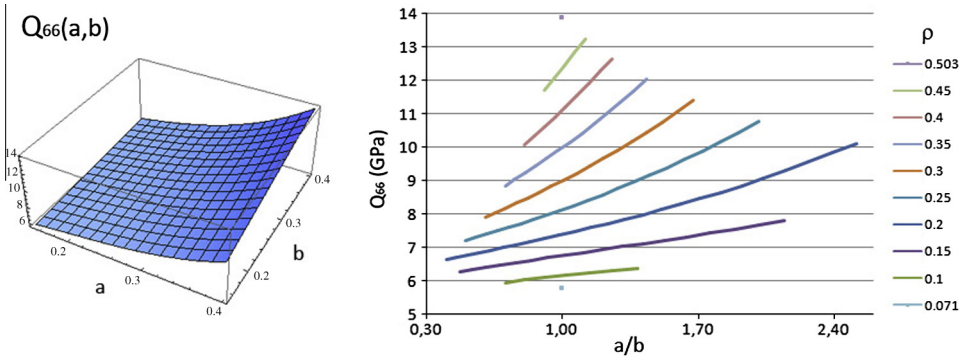

Fig. 3. Plots for the response surface developed for Q_{66}.

In terms of the quality of the fittings, the accuracy measures for all the response surfaces obtained were: for function values, $R^2 \simeq 1$ (the maximum value possible, indicating adequate fitting), *ARE* from 0% to 0.4% and *MRE* from 0.02% to 1.8%; for derivative values, R^2 from 0.95 to 1, *ARE* from 0.2% to 9.4% and *MRE* from 2% to 80%. All these values seem to be very adequate, except this last *MRE* for the derivatives. However, it has to be mentioned that biggest errors were found only in a few points. The checkings were made in both the IHS sampling points and also in a regular mesh of points not sampled for the fittings.

4. Discrete material optimization

Conceived upon multi-phase topology optimization ideas [32], the Discrete Material Optimization (DMO) [17,33] is a recently developed technique for purposes of material choice optimization, where a list of candidate materials is interpolated by appropriate functions to result in a variable material, in the following fashion:

$$\mathbf{C}(\mathbf{x}) = w_1(\mathbf{x})\mathbf{C}_1 + w_2(\mathbf{x})\mathbf{C}_2 + \cdots + w_j(\mathbf{x})\mathbf{C}_j + \cdots + w_n(\mathbf{x})\mathbf{C}_n = \sum_{j=1}^{n} w_j(\mathbf{x})\mathbf{C}_j \tag{5}$$

In the Eq. (5) above, the $\mathbf{C}_j$ matrices represent constitutive characteristics of discrete candidate materials in number n and the $w_j(\mathbf{x})$ are the interpolation functions, that can be seen as variable weights. This set of functions is defined to permit the weights to vary from 0 to 1 in terms of $\mathbf{x}$. The aim of this scheme is to represent the material $\mathbf{C}$ in a certain portion of the structure, and to define it by optimizing a certain parameter of the structure, like compliance or natural frequency for example. The $\mathbf{x}$ are taken as design variables, which clearly substitutes a discrete problem of choice of material by a continuous one in $\mathbf{x}$. A material is selected by pushing one of the weights to 1 (selecting the respective material) and the other weights to 0.

The candidates $\mathbf{C}_j$ may be any sort of material. A common application in the literature consists of distributing foam and unidirectional composite material in several orientations over plate/shell structures to form a sandwich-like optimal structure. Examples are [34], where buckling is taken into account, and [35], where vibration is considered.

In terms of interpolation functions $w_j(\mathbf{x})$, some schemes have been proposed very effectively, like the DMO4 and DMO5 [36], the most used. They basically consist of functions whose values vary from 0 to 1 within the $\mathbf{x}$ design space, and count with mechanisms that try to facilitate the convergence of the weights towards 0 and 1. For the DMO4, these functions have the form:

$$\mathbf{C}(\mathbf{x}) = \sum_{i=1}^{n} w_i(\mathbf{x})\mathbf{C}_i \quad w_i = (x_i)^p \prod_{j=1;j\neq i}^{n} \left[1 - (x_j)^p\right] \tag{6}$$

In the Eq. (6), the leading term with the x_i in the product is the one that pushes the w_i weight to 1, if this is the case according to the optimization in course. Contrariwise, the terms with the x_j push the w_i to zero, according to the problem convergence. The p parameter is a penalty whose goal is identical to that in the SIMP interpolation [6] in topology optimization: to penalize intermediate values of the weights in order to a desired 0–1 convergence. The DMO5 is a normalized version of these interpolation functions in order to have $\sum_{i=1}^{n} w_i = 1$, which may be interesting in terms of better material representation in certain problems.

Very recently the Shape Function with Penalization (SFP) scheme [37,38] was proposed. It is essentially a DMO-like scheme, but using as weighting functions some shape functions commonly found in interpolations of the finite element method [39]. For instance:

$$\mathbf{C}(\mathbf{x}) = \sum_{j=1}^{4} w_j(\mathbf{x})\mathbf{C}_j \quad \begin{matrix} w_1 = \left[\frac{1}{4}(1-x_1)(1-x_2)\right]^p & w_2 = \left[\frac{1}{4}(1+x_1)(1-x_2)\right]^p \\ w_3 = \left[\frac{1}{4}(1+x_1)(1+x_2)\right]^p & w_4 = \left[\frac{1}{4}(1-x_1)(1+x_2)\right]^p \end{matrix} \tag{7}$$

The functions defining the w_j in the brackets of Eq. (7) are bi-linear functions used in interpolating quantities in a four-node quadrilateral element, for example. They are in terms of x_1 and x_2, that could be seen as the so-called natural coordinates of the element and vary in the interval $-1 \leqslant x_1, x_2 \leqslant 1$. The definition of the w_j in SFP also counts with the p penalty parameter.

The advantage of the SFP in face of the DMO4/5 schemes is a reduction of design variables, in this case in the interpolation of four candidates. The DMO4/5 schemes would count with four variables while the SFP counts with two. However, its drawback is that the number of candidate materials is not so flexibly changed. The interpolation showed is valid only to four materials while the DMO4/5 schemes permit a full flexibility in this sense. Though, the SFP as shown is able to perform, for example, the interpolation of candidates defined from a unidirectionally fiber reinforced material at the $-45°/0°/45°/90°$ orientations, a lot common in composites design and manufacturing. This is the case of the problems to be dealt here and the SFP functions will be used in the discrete material optimization, in order to permit orientations choice for the variable material described in the latter section. Considering $\overline{\mathbf{Q}}$ the set of weighted constitutive parameters of a layer and $\overline{\mathbf{Q}}(a,b)_\theta$ the material constants $\overline{\mathbf{Q}}(a,b)$ oriented according to the θ angle, the interpolations employed are like the following:

$$\begin{aligned}\overline{\mathbf{Q}}(\mathbf{x},a,b) = {} & w_1(\mathbf{x})\,\overline{\mathbf{Q}}(a,b)_{-45} + w_2(\mathbf{x})\,\overline{\mathbf{Q}}(a,b)_0 + w_3(\mathbf{x})\,\overline{\mathbf{Q}}(a,b)_{45} \\ & + w_4(\mathbf{x})\,\overline{\mathbf{Q}}(a,b)_{90}\end{aligned} \tag{8}$$

5. The hierarchical approach

Fig. 4 depicts the optimization problem of interest together with a flowchart of the hierarchical optimization scheme employed here. The goal is to find, in each ith layer of a certain laminate, the microstructural parameters a_i, b_i and the volume fractions ρ_i to define the material properties $\mathbf{Q}_i$ and also the material orientations θ_i by determining the set of weights $w_j(\mathbf{x})$ in DMO interpolations like in Eq. (8). This is done in laminates subjected to specified load and boundary conditions, in order to increase stiffness. Mathematically, the problem of interest is the following:

$$\begin{aligned} \max_{w_j(\mathbf{x}),\,a_i,\,b_i} \ & \min_{\mathbf{u}\in\mathbf{u}_{adm}} \quad \frac{1}{2}\mathbf{u}^T\mathbf{K}\mathbf{u} - \mathbf{f}^T\mathbf{u} \\ & \rho_i = \pi a_i b_i \\ & \textstyle\sum_i \rho_i V_i \leqslant V_f \end{aligned} \tag{9}$$

In the Problem (9) above, it is considered that the total potential energy of a laminated structure discretized in finite elements is being maximized in the optimization parameters $w_j(\mathbf{x})$, a_i, b_i and minimized in the displacements $\mathbf{u}$, amongst the set of admissible displacements $\mathbf{u}_{adm}$. This minimization in $\mathbf{u}$ aims to find the equilibrium of the system while the maximization aims to increase the stiffness in $\mathbf{K}$. By noticing that the solution of $\mathbf{Ku} = \mathbf{f}$ (which is unique) assures the minimization in $\mathbf{u}$, it is possible to see that the problem is equivalent to a compliance minimization, or:

$$\begin{aligned} \min_{w_j(\mathbf{x}),\,a_i,\,b_i} \ & c = \mathbf{f}^T\mathbf{u} \\ & \mathbf{K}\mathbf{u} = \mathbf{f} \\ & \rho_i = \pi a_i b_i \\ & \textstyle\sum_i \rho_i V_i \leqslant V_f \end{aligned} \tag{10}$$

Therefore, this is a problem of finding the best set of weights w_j and also the best set of microstructural parameters a_i, b_i in order to minimize compliance (maximize stiffness). It is subjected to a resource constraint limiting the laminate total fiber volume V_f, where V_i and ρ_i are the ith lamina volume and fiber volume fraction respectively. This problem can be separated in two design interconnected subproblems: one in terms of the DMO weights and fiber volume fraction in each layer (macro-level design) and other in terms of the layers' microstructural parameters a_i, b_i (micro-level design). Thus, adding side constraints on the design variables, Problem (10) can be restated as a multi-level micro–macro design problem:

$$\begin{aligned} \min_{w_j(\mathbf{x}),\,\rho_i} \ & \min_{a_i,\,b_i} \quad c = \mathbf{f}^T\mathbf{u} \\ & \textstyle\sum_i \rho_i V_i \leqslant V_f \qquad \rho_i = \pi a_i b_i \\ & 0 \leqslant w_j(\mathbf{x}) \leqslant 1 \quad 0.15 \leqslant a_i, b_i \leqslant 0.4 \\ & \rho_{min} \leqslant \rho_i \leqslant \rho_{max} \end{aligned} \tag{11}$$

Note that both minimizations in Problem (11) are linked by the equality constraints $\rho_i = \pi a_i b_i$, correlating the fiber volume fraction with the microstructural fiber shape parameters a_i, b_i and thus fully linking the design problem at macro and micro-levels. Furthermore, the two levels exchange derivative information as will be described below. This is also clearly observed in the hierarchical optimization scheme,shown in the flowchart in Fig. 4, used to solve the optimization Problem (11).

Following the chart in Fig. 4, the optimization starts with a set of initial a_i, b_i, used to calculate the $\mathbf{Q}_i$ layer's matrices, and a set of initial $\mathbf{x}$ variables giving equal weights w_j for all the layer candidates, and thus not favoring any candidate orientation. With these data one can compute the overall composite material characteristics, calculate the stiffness global matrix $\mathbf{K}$ and solve the $\mathbf{Ku} = \mathbf{f}$ problem for equilibrium, in the current kth optimization iteration. Once the equilibrium solution $\mathbf{u}$ is obtained, the structural compliance c can be calculated and its derivatives evaluated from (see e.g. [40]):

$$\left.\frac{\partial c}{\partial a_i}\right|_k = -\mathbf{u}^T\frac{\partial \mathbf{K}}{\partial a_i}\mathbf{u} \quad \left.\frac{\partial c}{\partial b_i}\right|_k = -\mathbf{u}^T\frac{\partial \mathbf{K}}{\partial b_i}\mathbf{u} \quad \left.\frac{\partial c}{\partial w_j}\right|_k = -\mathbf{u}^T\frac{\partial \mathbf{K}}{\partial w_j}\mathbf{u} \tag{12}$$

In the sequence, it follows a compliance minimization at the micro-level, where only *one iteration* is performed by means of one unidirectional search in a_i, b_i. After that, the Lagrange multipliers λ_i of the micro-problem are evaluated (one per layer) giving us an estimate of the compliance c derivative with respect to each ρ_i as:

$$\left.\frac{\partial c}{\partial \rho_i}\right|_k = -\lambda_i^k \tag{13}$$

This result is based on the sensitivity theorem [41] of a minimization problem subjected to equality constraints, applied to the micro-level problem. This approximate derivative information is used at a macro-level minimization, where another unidirectional search is performed, giving a new set of weights w_j and a new set of ρ_i. After, these new ρ_i will be supplied to the subsequent micro-level minimization, where they act as limits defining the layer fiber volume fraction equality constraints. This iterative process is continued until the convergence criterion is satisfied.

It is useful mentioning that in the micro-level minimization, the equality constraint in optimal design Problem (11) is substituted by an inequality constraint, as shown in the flowchart of Fig. 4. This will ensure positive Lagrange multipliers thus giving to the derivative estimative in Eq. (13) a negative value, as would be expected for this compliance derivative with respect to fiber volume fraction. This change is irrelevant in terms of results, since the inequality constraint will always be active as compliance minimization requires total use of the available stiff material at the unit cell, but will improve accuracy on the Lagrange multiplier estimate.

In both the micro/macro-levels, the optimization solutions are obtained using the Conjugate Gradient method from the commercial software DOT v5.7 [42]. The Augmented Lagrangian Method (ALM) [43,40] is used to couple objective function and constraints.

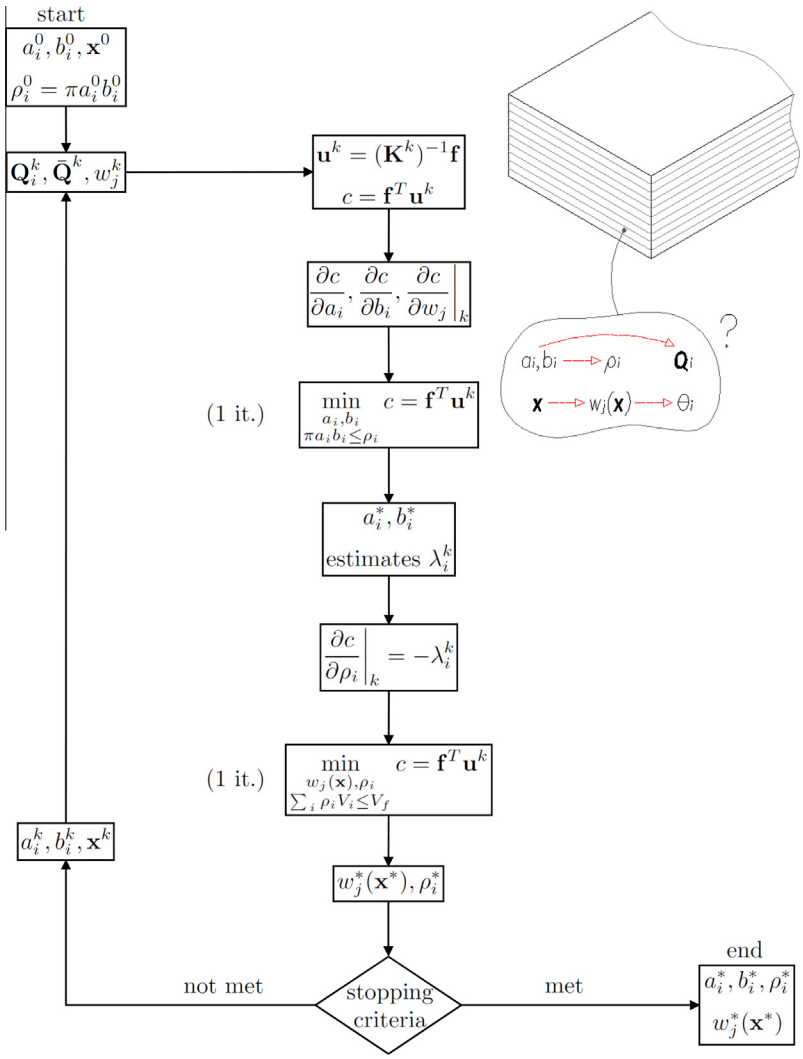

Fig. 4. Flowchart of the hierarchical optimization scheme employed.

Sequential Approximate Optimization concepts [18,19] are used throughout the iterations and the compliance is the quantity approximated in both levels. In the micro-level, conservative approximations in a_i, b_i are used and, in the macro-level, conservative approximations are used for the ρ_i while special direct approximations are used for the DMO weights part. The latter is a novel high quality type of DMO approximations based on intermediate variables which are explicit in the $w_j(\mathbf{x})$, and have been shown effective in rendering good material choice among the discrete candidates [44], in terms of weights well defined between 0 and 1.

6. Results

This section shows results obtained from the described methodology. Laminated plates are employed in the examples, a rectangular and also a square one, where the goal is to find optimal microstructural parameters and material orientations in each layer, for minimal compliance, considering several load and boundary conditions. For the rectangular plate, the dimensions of its mid-surface are 0.2×0.1 m and its total thickness is 0.7 mm, with the laminate counting with seven layers of 0.1 mm each. In this case, the loadings include bending, membrane-bending, pure shear, torsion and shear-torsion, as depicted in Figs. 5–9. This plate is considered clamped at the opposite edge where the loads are applied in all the loading cases. Regarding to the square plate, it has the same thickness and laminae characteristics as the rectangular one, but its mid-surface measures 0.2×0.2 m. In this case, the boundary conditions applied include two neighbor edges clamped and bending loads at the two reminiscent edges, as shown in Fig. 10.

All the cases are analyzed using the commercial finite elements software ABAQUS, using *S4* shell elements. In the case of the rectangular plate, the meshes have 20×10 elements and in the case of the square plate, 20×20. First the results for the rectangular plate will be discussed and then the square plate ones.

6.1. Rectangular plate

From initial tests in the cases of bending and membrane-bending, the preponderant stress component in the stress states of the rectangular plate layers is the direct stress σ_{11}. In the cases of pure shear, torsion and shear-torsion, the preponderant stress component is the in-plane shear stress τ_{12}. These observations were well expected. According to the Reissner–Mindlin plate theory, all the stress components in the plane of the layers $(\sigma_{11}, \sigma_{22}, \tau_{12})$ have a linear piecewise distribution over the laminate layers and the corresponding strains $(\epsilon_{11}, \epsilon_{22}, \gamma_{12})$ vary linearly over the hole thickness of the plate. Such behavior was observed in the results obtained and is also reported in the ABAQUS manual with respect to the *S4* element.

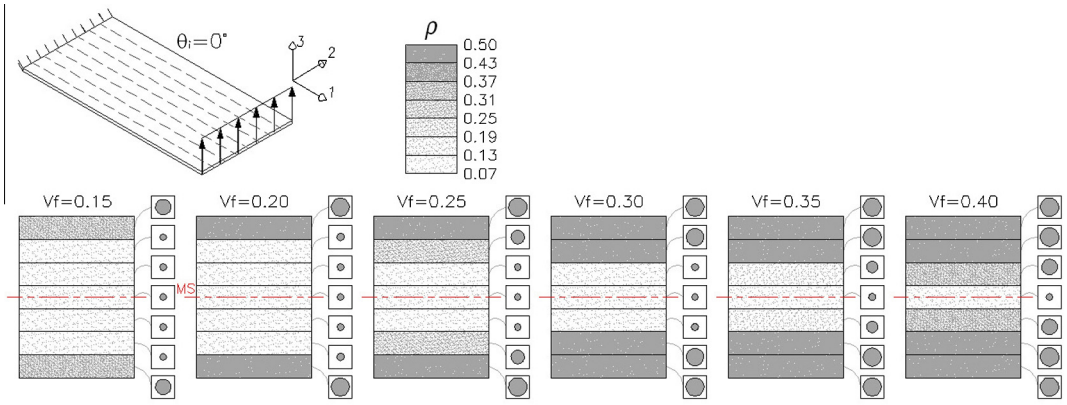

Fig. 5. Rectangular plate bending case for several volume fractions V_f. The neutral surface *NS* coincides with the plate mid-surface *MS*.

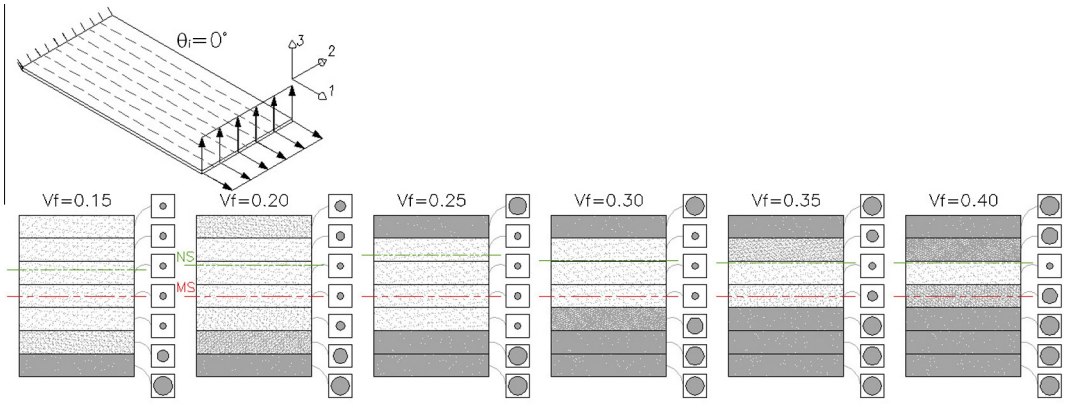

Fig. 6. Rectangular plate membrane-bending case for several volume fractions V_f. The neutral surface *NS* is shifted in relation to the plate mid-surface *MS*.

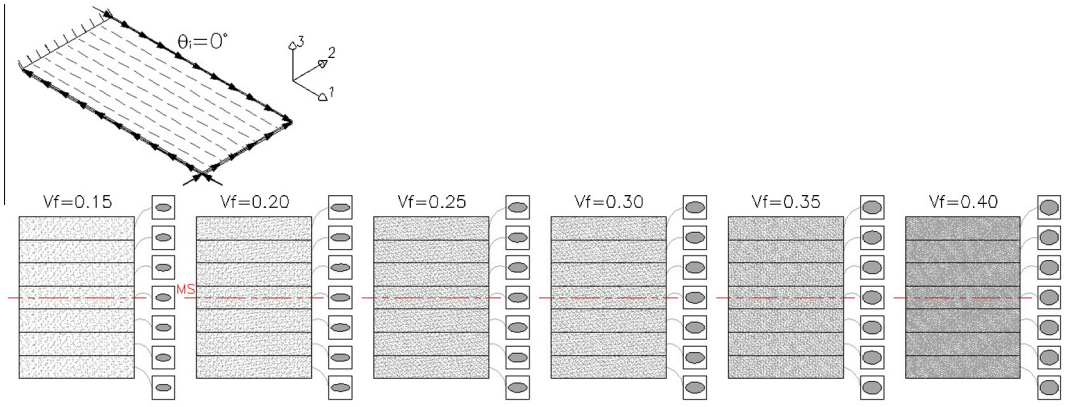

Fig. 7. Rectangular plate pure shear case for several volume fractions V_f. *MS* is the plate mid-surface.

In terms of optimization, the objective here is to solve the Problem (11) (minimizing compliance) by the scheme in Fig. 4, for several admissible volume fractions, namely $V_f = 0.15, 0.20, \ldots, 0.40$. The design starting point adopted in terms of microstructure is $a_i = b_i = 0.20$ for all the layers in practically all the cases, except from a few runs where $a_i = b_i = 0.15$ was necessary to a better design convergence. Therefore, fibers of circular cross-section were initially considered. Also, it is worthwhile to mention that these initial designs are admissible, with fiber volume fractions of $V_f \approx 0.125$ and $V_f \approx 0.071$ respectively.

Regarding to initial material orientations, the DMO4 and SFP interpolations in Eqs. (6) and (7), when used, had initial variables x_i set in such a way that the weights w_i had equal values amongst the candidate orientations in Eq. (8), in all the laminate layers, which is done to not favor any candidate from the beginning of the optimization. In the DMO4, this is done by setting $x_i = 0.5$ and in the SFP by imposing $x_i = 0$. The penalty in the DMO4 interpolations was always set $p = 2.5$ and in the SFP $p = 3$ was used. Although the compliance and variables variation was checked, the stopping criteria adopted was the maximum number of k iterations for the iterative scheme in Fig. 4.

In Fig. 5, it is possible to see the results obtained for the rectangular plate bending case, that were achieved in runs of $k = 100$–170 iterations. In this case, the stresses σ_{11} were found to be the preponderant stress components among those calculated over the layers. Moreover, due to the fact that bending is the dominant effect, it

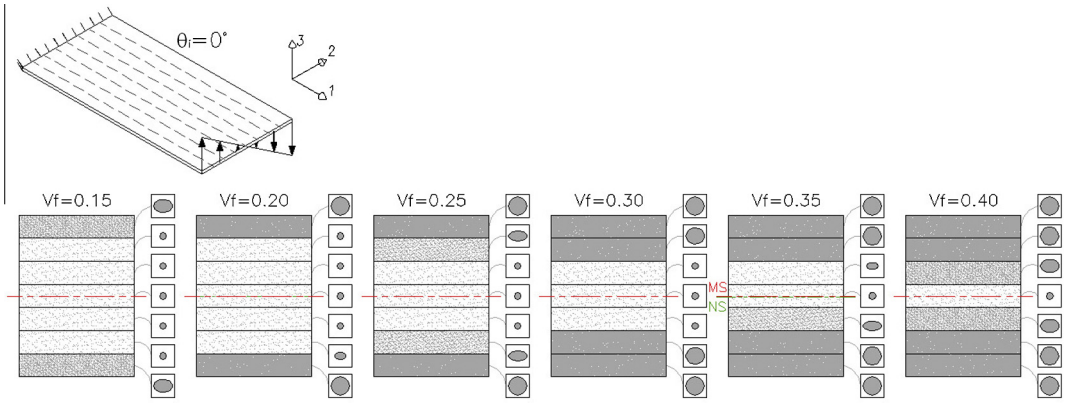

Fig. 8. Rectangular plate torsion case for several volume fractions V_f. The neutral surface *NS* coincides with the plate mid-surface *MS* in all cases, except $V_f = 0.20, 0.35$.

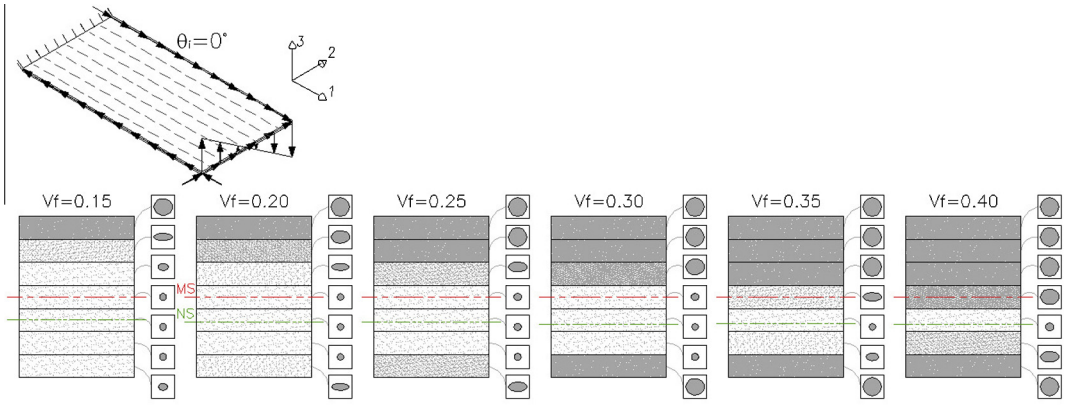

Fig. 9. Rectangular plate shear-torsion case for several volume fractions V_f. The neutral surface *NS* is shifted in relation to the plate mid-surface *MS*.

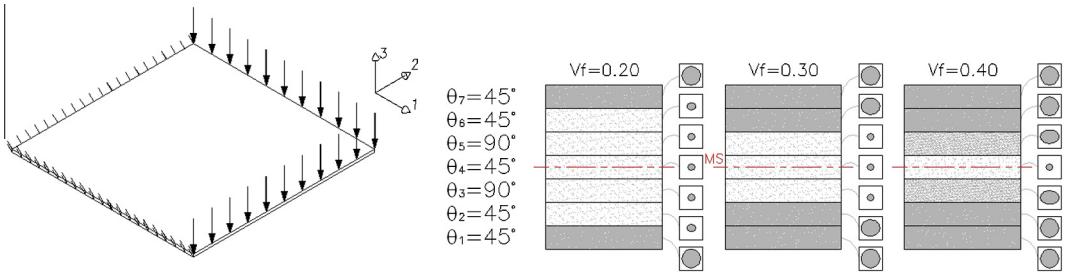

Fig. 10. Square plate bending case for volume fractions $V_f = 0.20$, 0.30 and 0.40. *MS* is the plate mid-surface.

is expected the outer layers are the most loaded ones, due to the anti-symmetric distribution of stresses/strains over the plate thickness, with the neutral surface *NS* of the plate coinciding with its mid-surface *MS*. Thus, this loading feature led to a characteristic material distribution for the different cases with several admissible fiber volume fractions: the outer layers tend to have as much fiber material as possible, in accordance to V_f, letting the remaining stiff material to the subsequent inner layers. This dictated the symmetrical choice of the ρ_i over the layers. In terms of the results for the a_i, b_i, the shape of the fibers ended up practically circular. This can also be confirmed from the results shown in Table A.2 of Appendix A, where the numerical results for these design variables are included. The shape of the fibers remained circular because the variable stiffness Q_{11} in the 1 direction is not sensitive to the fiber cross-sectional shape, as described earlier with the aid of Fig. 2. The orientation chosen for all the layers was $\theta_i = 0°$ with respect to the 1 direction, due to the preponderant σ_{11} stress. This selection was made by converging in all the layers the weights $w_2 = 1$ and $w_1 = w_3 = w_4 = 0$ in Eq. (8). In this case, the SFP interpolation scheme was used.

It is worthwhile to mention that a pure tension case was also run, in the same fashion of the bending case depicted, obtained by just changing the bending load in Fig. 5 to a in-plane one. This case rendered optimal designs with constant distributions of ρ_i, orientations $\theta_i = 0°$ and equal circular fibers over the layers, according to the V_f allowed, as could be expected.

Now, a superposition of the transverse bending load with an in-plane tension load was used to render a new case, called here membrane-bending and shown in Fig. 6. Once again, a preponderant σ_{11} stress component could be expected in the layers, but this time the anti-symmetry of the stresses/strains distribution in relation to the plate mid-surface is lost, in comparison to the bending

case, with the plate neutral surface not coincident with its mid-surface anymore. Moreover, due to the loads applied as seen in Fig. 6, this neutral surface is expected to be shifted somewhere on the upper half of the laminate, having the lower laminae more loaded. It can be observed that this characteristic clearly influenced the results obtained in this case. However, the trend of having more fiber material in the most loaded layers was kept. This pattern evolved as expected when the available fiber volume fraction increased. The results for a_i, b_i (see again Table A.2) showed, once more, that the fibers' cross-section were practically circular, in accordance with the most required stiffness Q_{11}. The orientations chosen for all the layers was again $\theta_i = 0^\circ$ using the SFP interpolation, and the number of iterations was $k = 100$–120 over the several cases.

In the following, the pure shear case is considered, as shown in Fig. 7. In this case, the loading and boundary conditions are assumed to cause a pure shear stress state in all the elements of the finite elements mesh considered for the plate. Thus, the preponderant stress component is expected to be the shear τ_{12}, which highlights that the stiffness variation with a_i, b_i expected for this problem is mainly governed by the Q_{66} laminae stiffness component in Eq. (3). This variation was depicted in Fig. 3 showing the influence of this stiffness in the shape of the fibers. As earlier described, for the several admissible V_f, the initial designs were taken as uniform distributions of volume fractions and circular fiber cross-sections in all the layers of the laminates. This time, however, it is possible to see that the final designs converged to fiber cross-sections of elliptical shape, with the highest a_i/b_i ratio as possible, tough maintaining uniform distributions of ρ_i over the layers. This can be explained by the fact that the highest Q_{66} that may be obtained for a certain ρ_i is the one with the highest a_i/b_i as possible, which can be confirmed in Fig. 3, giving the maximum stiffness to the layers. These results are again summarized in Table A.2. In terms of laminae orientations, the DMO weighting scheme selected the $\theta_i = 0^\circ$, in respect to the 1 direction, in all the layers. The interpolation used was the DMO4. This result may look strange in terms of optimal orientations, since it is expected that an orthotropic material should be oriented with the principal strains directions in an optimal design, which in this case are mostly placed at 45° with the 1 axis. However, the variable material being used here can be classified as "strong in shear" according to [45]. Due to this, an optimal orientation of 45° with respect to the principal strains' directions may be predicted for this orthotropic material, resulting in an optimal orientation of $\theta_i = 0^\circ$ with the 1 axis for the case. The orientation $\theta_i = 90^\circ$ with 1 could also be shown as an optimal solution, but the clamped boundary condition used here gave a slight advantage to the $\theta_i = 0^\circ$. Approximately $k = 50$ iterations were performed to obtain the designs shown.

Now, the rectangular plate torsion case shown in Fig. 8 is considered. In this case, the preponderant stress evaluated was the shear τ_{12} again, but now counting also with contributions of other stress components over the layers, due to the bending caused in the plate loaded edge. The distributions of the in-plane stresses over the layers are also expected to be piecewise linear with the outer laminae more loaded. These characteristics led to optimal designs with higher ρ_i values in the outer layers. Depending on the total fiber (V_f) available the trend again is to put as much fiber material as possible in the outer layers and then distribute the remaining material by the subsequent layers. This time, however, in the layers with intermediate ρ_i values (i.e. not hitting the bounds $0.071 < \rho_i < 0.502$), the elliptical shape of the fibers plays a significant role. The fibers assumed elliptical cross-section, converging always to the biggest a_i/b_i as possible, in order to maximize the mainly influent stiffness Q_{66}, as previously observed in the pure shear case. The final designs showed to be symmetric except in the cases with $V_f = 0.20$ and $V_f = 0.35$, leading to a slight shift in the neutral surface in relation to the plate mid-surface in these cases. Further tests comparing them with the possibly expected symmetric designs showed that they are local minimum design points a little worse than those symmetric. The layer orientation chosen was $\theta_i = 0^\circ$ for all of them, using SFP. The number of iterations ranged from $k = 100$ to 450 in order to obtain the designs shown. This increase in the number of iterations in relation to the other loading cases may be related to the different microstructural solutions. Results' details are shown in Table A.2.

The shear-torsion case is the last one of the rectangular plate to be presented. It is seen in Fig. 9 and couples the pure shear and torsion loads in order to obtain a loading case where the shear stress τ_{12} is still preponderant in the layers, but trying to deviate on purpose the optimal material distribution from a symmetric disposal, in the same fashion as in the membrane-bending case. This time, due to the loads considered, the upper layers became the most loaded, whose influence is seen in the results shown. The fiber material filling in the layers followed the patterns found in the bending, membrane-bending and torsion cases: the biggest values of fiber volume fractions ρ_i in the most loaded layers and then the remaining stiff material is distributed subsequently in the other layers, according to V_f. Therefore, in this case, the fiber material distribution over the layers is indeed non-symmetric. The cross-sections of the fibers followed the trend presented in the torsion case: if not in the upper or lower limit for ρ_i, the fiber shapes converged to ellipses with the greatest a_i/b_i ratio as possible, due to the main stiffness in the problem to be the Q_{66} in Fig. 3. The orientations of all the layers converged to $\theta_i = 0$ (using SFP) and the number of iterations ranged from $k = 250$ to 350 to obtain the designs presented, showing that the microstructure convergence also took more time in this case.

In order to evaluate the improvements achieved by the hierarchical optimization applied to the rectangular plate cases described, the compliances found in the optimized designs were compared with compliance values calculated from designs with uniform distributions of ρ_i through the layers and a_i, b_i defining fibers of circular cross-sections. These test-designs are shown in the end of Table A.2 (Appendix A), and were used in a direct comparison in relation to the designs obtained in all the cases represented in Figs. 5–9, that had influence of distinct distributions of ρ_i and cross-sectional shapes for the fibers over the layers. The orientations θ_i found were maintained. This emulates a situation where a designer of composite laminates has no choice in terms of shape of the fibers and also in terms of being able to vary the volume fraction over the layers.

Thus, this assessment showed that the gains due to the use of varying ρ_i and a_i, b_i in the bending case were about 20–59% in terms of compliance (in the sense of a higher stiffness). In the membrane-bending case, these gains were about 19–57%. In the pure shear case, the gains obtained were around 14–37%. In the torsion case, gains in the order of 21–49% were found. Finally, in the shear-torsion case, the gains achieved were from 21% to 53%. All these improvements depended on the total volume fractions V_f, with the tendency of the highest gains to be found in the cases with the lowest V_f, in general.

6.2. Square plate

The square plate case is an additional case of study with the same goals as the rectangular plate one, and consists of a bending case with boundary and load conditions according to Fig. 10. The objective is again to minimize compliance in the same terms as the previous cases, according to the Problem (11), but now for total volume fractions of $V_f = 0.20$, 0.30 and 0.40. The plate has the same lay-up characteristics as in the rectangular plate cases.

The design starting points concerning to the microstructure of the layers again consider circular fibers with $a_i = b_i = 0.20$, for all the seven layers as used before. Regarding to choice of material orientations, the DMO4 interpolation in Eq. (6) was used with $p = 2.5$ and initial variables set to $x_i = 0.5$, meaning that all the four candidate orientations started with the same initial weighting, not prevailing any of the orientations beforehand and following the scheme adopted in the rectangular plate cases. The stopping criteria chosen was also the same as before: a k number of iterations.

This time, however, some initial assessments showed that none of the in-plane stress components σ_{11}, σ_{22} or τ_{12} can now be elected as preponderant over the plate layers: all of them have a considerable magnitude in this case. Besides, it was shown in Fig. 3 that the Q_{66} stiffness has influence of the cross sectional shape of the fibers and, moreover, it can be shown that the Q_{12} and Q_{22} stiffnesses (all in the Eq. (3)) also have a similar influence of the shape of the fibers, increasing with the a/b ratio. If these material properties are transformed according to some orientation, this influence is also preserved. Therefore, it is expected that the fibers' shapes have some influence in this problem.

The optimized results obtained with about $k = 250$–350 iterations are also shown in Fig. 10. From a first inspection, it is noticed that this time the orientations θ_i over the layers converged to values different from zero degree. They assumed $\theta = 45°$ or $\theta = 90°$ with the 1 axis by selecting, respectively, $w_3 = 1$ or $w_4 = 1$ in the DMO4 interpolations used, following Eq. (8). The same optimal orientations shown in Fig. 10 were obtained for all the V_f considered and were a posteriori tested to check if this was indeed a good design for orientations, showing positive results.

In terms of layers' material design, the optimal results show a similar fiber material distribution over the layers of the plate in comparison to the rectangular plate cases presented: more stiff material in the more loaded laminae (in this case the outer ones), as much as possible as the V_f considered permits, and then the remaining stiff material distributed in the subsequent inner layers. Moreover, as this bending case presents the neutral surface of the plate coinciding with its mid-surface, the ρ_i volume fractions distributions found were symmetrical. Regarding to the cross-sections of the fibers, they assumed circular and elliptical shapes over the layers. The latter ones for intermediate values of ρ_i. In other words, the a_i/b_i ratio followed the trend of reaching the biggest possible value for the layer fiber volume fraction ρ_i, as a consequence of the dependence of Q_{12}, Q_{22} and Q_{66} on it (see Fig. 3 and Section 3), since all the in-plane stresses are important. The numerical results for the a_i, b_i are depicted in Table A.2.

To finalize the discussion of the square plate case, the obtained optimal microstructural designs were also compared with uniform circular fiber microstructural designs counting, exactly as performed to the rectangular plate cases. This was done for $V_f = 0.20$, 0.30 and 0.40, keeping the orientations found by optimization. These microstructure uniform test-designs results are shown in Table A.2. This comparison showed improvements on the compliance value (maximization of stiffness) from 21% to 57%. The same order of improvement was found in the rectangular plate case.

7. Design evaluation in terms of microstructural stresses

The optimal results in the last Section 6 were obtained by the minimization of compliance in laminated composite plates. In this section, one of these designs is evaluated in terms of assessing the influence of the variation of fiber cross sectional shapes in the microstructural stresses over its laminae. The aim is to verify

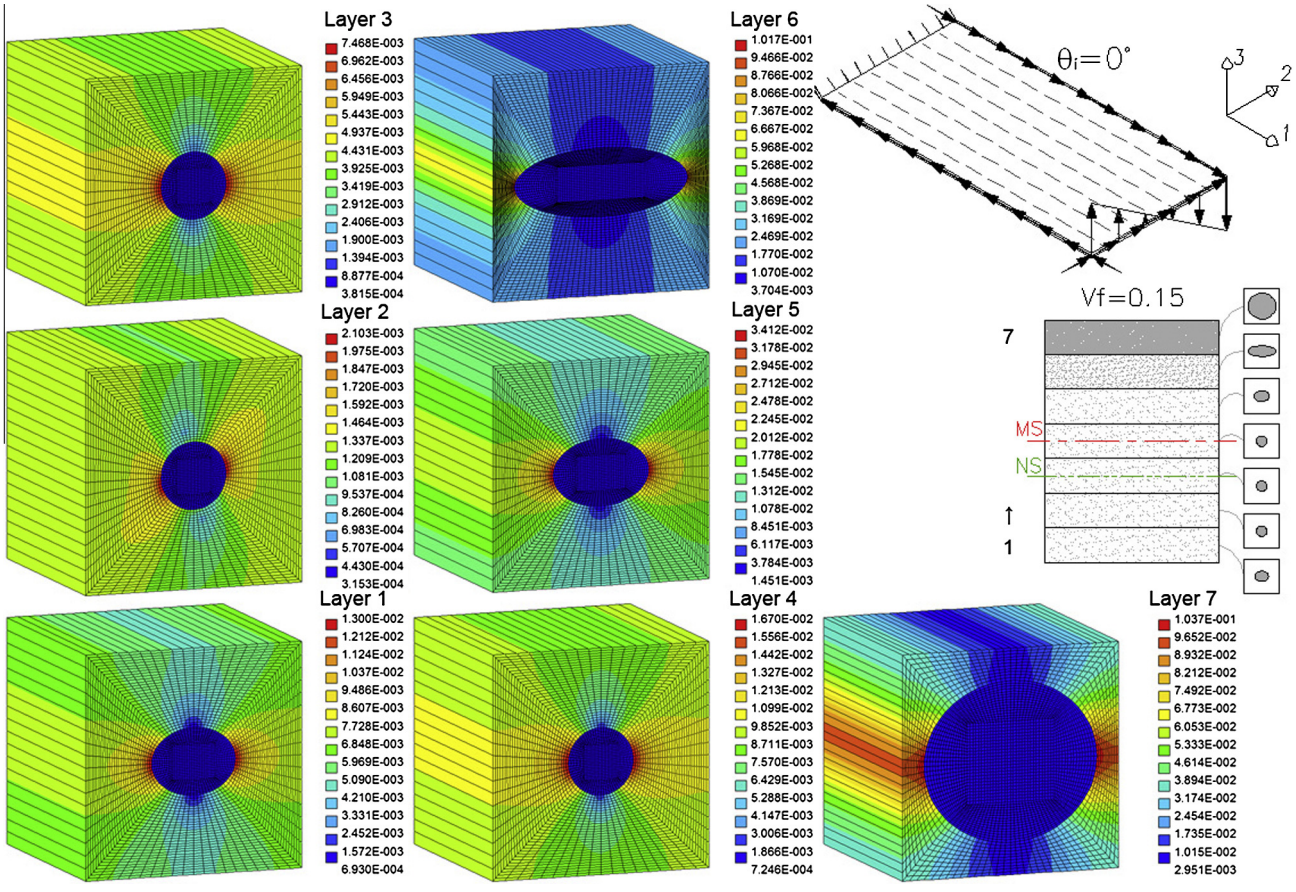

Fig. 11. Failure parameters in the optimized design obtained for the rectangular plate in the shear-torsion case with $V_f = 0.15$.

wether the elliptical fibers obtained in several optimization cases may lead to undesired stress concentrations in the composites' microstructure. The design chosen to illustrate this point is the one from the rectangular plate shear-torsion case with $V_f = 0.15$, or the first depicted in Fig. 9. It is compared to the case of the same plate under the same load and boundary conditions but with constant microstructural design over its layers, with circular fiber cross sections and respecting the total fiber volume fraction $V_f = 0.15$; this microstructural design represents the ones commonly found in practice and is detailed among the uniform test-designs of Table A.2.

The stresses in the level of material microstructure are here obtained from the asymptotic homogenization theory, by considering the displacement test fields χ_r^{km} from Eq. (2) as:

$$\sigma_{ij} = E_{ijkm}\left(\delta_{kr}\delta_{ms} - \frac{\partial \chi_k^{rs}}{\partial y_m}\right)\epsilon_{rs}^0 \tag{14}$$

In the Eq. (14) above, the σ_{ij} are the micro-stresses, δ_{ij} are Kronecker deltas and ϵ_{rs}^0 is the macroscopic (average) strain field. For more details, see [7]. The σ_{ij} results represent the tridimensional stress states varying throughout the unit cell of Fig. 1, with the stress field respecting the material discontinuity between fiber and matrix and also periodicity conditions. Here, the methodology used for obtaining such stresses is based in the software POSTMAT [7].

Then, to assess the stress level, the Drucker–Prager and the von Mises yield criteria [46] are used. The first is used to evaluate failure in the matrix, since it is able to consider different yield limits under compression and tensile stresses for a material, which is important for polymers, in this case an epoxi resin. Enven though failure is expected to occur first in the matrix, the von Mises yield criteria is also monitored in the fiber. Similar methodologies for evaluation of microstructural stresses in fiber composites can be seen in [47–49], inclusive to consider damage onset and evolution. The Drucker–Prager criteria is used here in the following normalized form, where (matrix) failure is admitted when:

$$\frac{\alpha_m I_1 + \sqrt{J_2}}{k_m} = 1 \tag{15}$$

In the last equation, I_1 is known as the first invariant of a stress state and the J_2 is the second deviatoric stress invariant. The latter can be given in terms of I_1 and I_2, the second invariant of a stress state, as $J_2 = (1/3)(I_1^2 + 3I_2)$. The parameters α_m and k_m are material constants, related to the cohesion yield stress c_m and the angle of internal friction ϕ_m as follows:

$$\alpha_m = \frac{2\sin\phi_m}{\sqrt{3}(3+\sin\phi_m)} \quad k_m = \frac{6c_m\cos\phi_m}{\sqrt{3}(3+\sin\phi_m)}$$

$$\phi_m = \arcsin\left(\frac{X_c - X_t}{X_c + X_t}\right) \quad c_m = \frac{\sqrt{X_c X_t}}{2} \tag{16}$$

In the last Eq. (16), X_c and X_t are the compressive and tensile yield strengths of a material, respectively. If $X_c = X_t$, the Drucker–Prager yield criterion in Eq. (17) reduces to the von Mises criterion, with $\phi_m = \alpha_m = 0$ and $k_m = X_t/\sqrt{3}$. This fact is used here considering that (fiber) failure occurs when:

$$\frac{\sqrt{J_2}}{k_m} = 1 \tag{17}$$

The material yield parameters employed are $X_{tM} = 80$ MPa and $X_{cM} = 120$ MPa in the matrix and $X_{tF} = 2150$ MPa in the fiber [47], considering epoxi resin matrix and glass fiber. Figs. 11 and 12 show

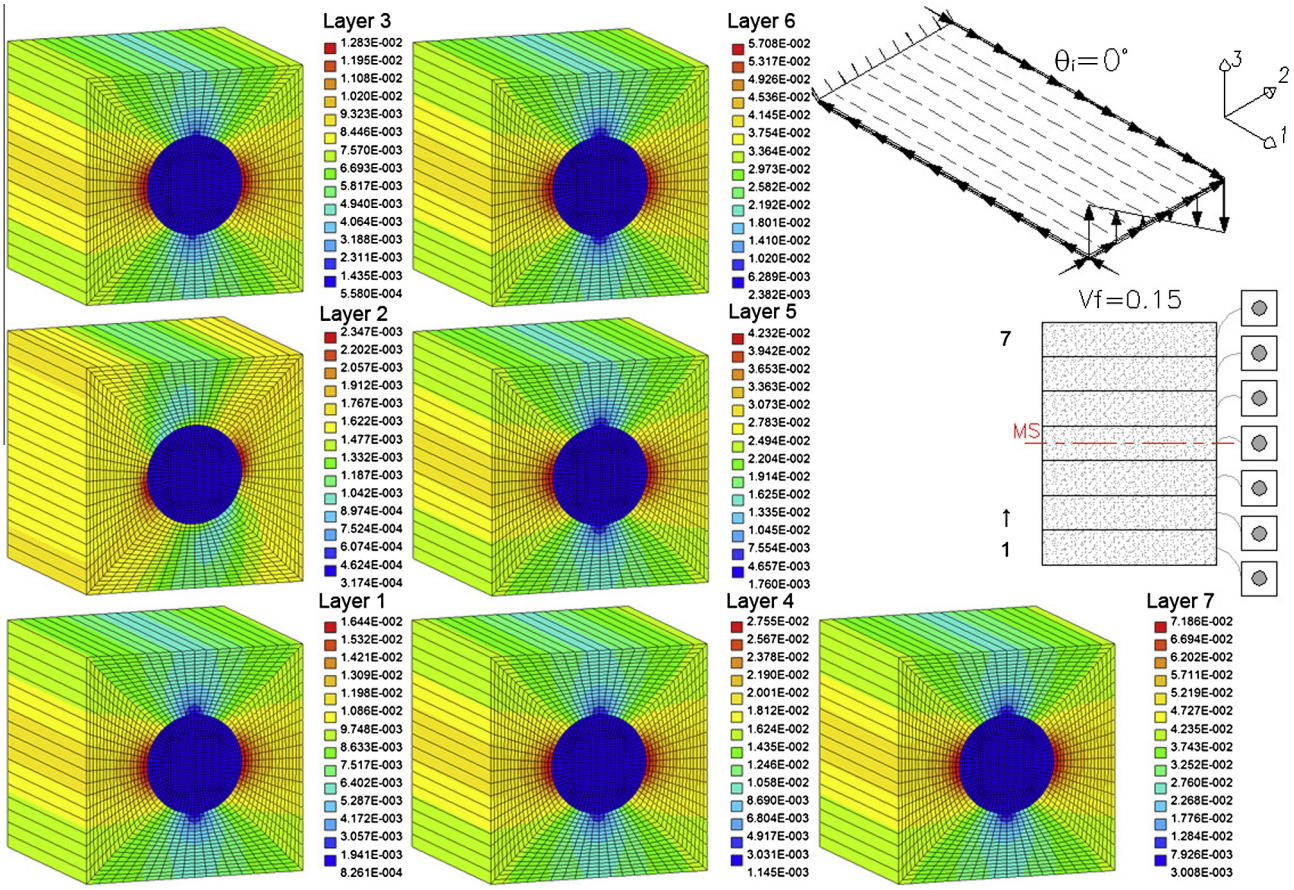

Fig. 12. Failure parameters in a uniform design for the rectangular plate in the shear-torsion case with $V_f = 0.15$.

Table 1
Maximum Drucker–Prager failure indices in the matrix (from Figs. 11 and 12).

Layer	Optimized design	Uniform design	Opt./unif. ratio
7	1.037×10^{-2}	7.186×10^{-2}	0.144
6	1.017×10^{-1}	5.708×10^{-2}	1.782
5	3.412×10^{-2}	4.232×10^{-2}	0.806
4	1.670×10^{-2}	2.755×10^{-2}	0.606
3	7.468×10^{-3}	1.283×10^{-2}	0.582
2	2.103×10^{-3}	2.347×10^{-3}	0.896
1	1.300×10^{-2}	1.644×10^{-2}	0.791

the results of the failure parameters for the optimized and uniform microstructures, respectively. These parameter were computed assuming that the loads considered were 6000 N/m for the in-plane shear and a linear variation of 2400 to −2400 N/m in the torsion load. The stresses in the microstructures are evaluated using the "macro" average stress provided by the ABAQUS solutions for the center point of each layer thickness, close to the clamped side and the plate center line.

The associated maximum failure indices in each layer are presented on Table 1 for both the optimized and uniform microstructures. All values are well bellow 1, and from their ratio it is possible to notice that the optimized design is in general better except for layer 6, where an elliptical fiber exists. This shows that fibers with elliptical shape may introduce undesired stress concentrations in the matrix, close to the fiber cross-section highest curvature points. However, by the numerical value of the failure index in the layer 6, it can be seen that the lamina is still far from failure at the sampled point.

Therefore, the fibers with cross-sections different from circular were useful in increasing stiffness in this case, but care must be taken with stress concentrations existing at the boundary between matrix and the fibers, in order to decide substituting circular fibers for optimized ones.

8. Conclusions

This work applied the hierarchical optimization in the design of laminated fiber composites, with the goal of simultaneously design macrostructural and microstructural levels of structures, in terms of plies orientations and fiber volume fractions and also in terms of fiber cross-sectional shapes, respectively. The DMO approach was successfully coupled with the multi-scale methodology in order to choose layers' orientations in the macro-level.

The results showed that laminate plate stiffness could be improved either finding optimal ply orientation, fiber volume fraction or fiber shape. Problems where in-plane shear stresses where preponderant or of the same order of magnitude as normal stresses in the ply laminas favored elliptical fiber shapes. Moreover, the asymptotic homogenization approach, employed to form the response surfaces of stiffness parameters of a lamina, could be also used to calculate stresses in the micro-level of the layers. This allowed the use of appropriate failure criteria in the laminae microstructure, showing that elliptical cross-sections may introduce undesired stress concentrations in the matrix. These stress concentrations at the microstructure level, although not so critical in the cases analyzed (see Table 1), are a very important design issue that should be the focus of future developments of this work.

The method here applied to elliptical fibers can easily be extended to more complex fiber cross-sections, giving the designer the possibility to include the more recent developments achieved in fiber production, namely in alternative cross section shapes.

Acknowledgements

We are thankful to the financing of this work by the CAPES Aux-PE-FCT 243/2011 Project. Also to Vanderplaats Research and Development, Inc. by the gentle cession of a DOT v5.7 research license. The finite element results were drawn with FEPlot 3.1.19, by the MUST and ODESSY teams, Aalborg University, Denmark.

Appendix A. Designs' details

Table A.2 shows details for the a_i, b_i fiber shape variables found in all the optimization cases depicted in Figs. 5–10. The ρ_i variables are omitted since the optimized designs obtained presented the equality constraints in Problem (11) well respected. They ended up active (close to zero) so the ρ_i can be easily obtained by $\rho_i = \pi a_i b_i$. In the end of the table, the uniform test-designs used to assess all the optimized ones are also shown.

Table A.2
Designs in terms of the a_i, b_i for the referred cases.

Layer	$V_f = 0.15$		$V_f = 0.20$		$V_f = 0.25$		$V_f = 0.30$		$V_f = 0.35$		$V_f = 0.40$	
	a_i	b_i	a_i	b_i	a_i	b_i	a_i	b_i	a_i	b_i	a_i	b_i
	Rectangular plate bending											
7	0.332	0.333	0.400	0.400	0.400	0.400	0.400	0.400	0.400	0.400	0.400	0.400
6	0.150	0.150	0.168	0.168	0.290	0.292	0.372	0.377	0.400	0.400	0.400	0.400
5	0.150	0.150	0.150	0.150	0.150	0.150	0.150	0.150	0.242	0.243	0.337	0.339
4	0.150	0.150	0.150	0.150	0.150	0.150	0.150	0.150	0.152	0.153	0.150	0.150
3	0.150	0.150	0.150	0.150	0.150	0.150	0.150	0.150	0.242	0.243	0.337	0.339
2	0.150	0.150	0.168	0.168	0.290	0.292	0.372	0.377	0.400	0.400	0.400	0.400
1	0.332	0.333	0.400	0.400	0.400	0.400	0.400	0.400	0.400	0.400	0.400	0.400
	Rectangular plate membrane-bending											
7	0.150	0.150	0.248	0.248	0.383	0.384	0.400	0.400	0.400	0.400	0.400	0.400
6	0.150	0.150	0.181	0.182	0.150	0.150	0.150	0.150	0.256	0.257	0.349	0.351
5	0.150	0.150	0.150	0.150	0.150	0.150	0.150	0.150	0.162	0.162	0.150	0.150
4	0.150	0.150	0.150	0.150	0.150	0.150	0.150	0.150	0.220	0.220	0.325	0.327
3	0.150	0.150	0.207	0.207	0.150	0.150	0.348	0.350	0.400	0.400	0.400	0.400
2	0.248	0.248	0.318	0.318	0.400	0.400	0.400	0.400	0.400	0.400	0.400	0.400
1	0.400	0.400	0.400	0.400	0.400	0.400	0.400	0.400	0.400	0.400	0.400	0.400
	Rectangular plate pure shear											
7	0.318	0.150	0.400	0.159	0.400	0.199	0.400	0.239	0.400	0.279	0.400	0.318
6	0.318	0.150	0.400	0.159	0.400	0.199	0.400	0.239	0.400	0.279	0.400	0.318
5	0.318	0.150	0.400	0.159	0.400	0.199	0.400	0.239	0.400	0.279	0.400	0.318

(*continued on next page*)

Table A.2 (*continued*)

Layer	$V_f = 0.15$		$V_f = 0.20$		$V_f = 0.25$		$V_f = 0.30$		$V_f = 0.35$		$V_f = 0.40$	
	a_i	b_i	a_i	b_i	a_i	b_i	a_i	b_i	a_i	b_i	a_i	b_i
4	0.318	0.150	0.400	0.159	0.400	0.199	0.400	0.239	0.400	0.279	0.400	0.318
3	0.318	0.150	0.400	0.159	0.400	0.199	0.400	0.239	0.400	0.279	0.400	0.318
2	0.318	0.150	0.400	0.159	0.400	0.199	0.400	0.239	0.400	0.279	0.400	0.318
1	0.318	0.150	0.400	0.159	0.400	0.199	0.400	0.239	0.400	0.279	0.400	0.318
	Rectangular plate torsion											
7	0.400	0.277	0.400	0.400	0.400	0.400	0.400	0.400	0.400	0.400	0.400	0.400
6	0.150	0.150	0.150	0.150	0.400	0.212	0.400	0.346	0.400	0.400	0.400	0.400
5	0.150	0.150	0.150	0.150	0.150	0.150	0.150	0.150	0.251	0.150	0.400	0.287
4	0.150	0.150	0.150	0.150	0.150	0.150	0.150	0.150	0.150	0.151	0.150	0.150
3	0.150	0.150	0.150	0.150	0.150	0.150	0.150	0.150	0.400	0.200	0.400	0.286
2	0.150	0.150	0.238	0.150	0.400	0.212	0.400	0.357	0.400	0.400	0.400	0.400
1	0.400	0.277	0.400	0.400	0.400	0.400	0.400	0.400	0.400	0.400	0.400	0.400
	Rectangular plate shear-torsion											
7	0.400	0.357	0.400	0.400	0.400	0.400	0.400	0.400	0.400	0.400	0.400	0.400
6	0.400	0.154	0.400	0.266	0.400	0.400	0.400	0.400	0.400	0.400	0.400	0.400
5	0.222	0.150	0.375	0.150	0.400	0.211	0.400	0.341	0.400	0.400	0.400	0.400
4	0.150	0.150	0.151	0.150	0.169	0.150	0.162	0.150	0.400	0.180	0.400	0.329
3	0.150	0.150	0.150	0.150	0.156	0.153	0.150	0.150	0.154	0.151	0.177	0.166
2	0.151	0.150	0.151	0.150	0.154	0.151	0.154	0.152	0.259	0.165	0.400	0.227
1	0.194	0.150	0.368	0.150	0.400	0.202	0.400	0.355	0.400	0.400	0.400	0.400
	Square plate bending											
7			0.400	0.400			0.400	0.400			0.400	0.400
6			0.193	0.150			0.400	0.351			0.400	0.400
5			0.150	0.150			0.150	0.150			0.400	0.286
4			0.150	0.150			0.150	0.150			0.150	0.150
3			0.150	0.150			0.150	0.150			0.400	0.286
2			0.196	0.150			0.400	0.351			0.400	0.400
1			0.400	0.400			0.400	0.400			0.400	0.400
	Uniform test-designs											
7	0.219	0.219	0.252	0.252	0.282	0.282	0.309	0.309	0.334	0.334	0.357	0.357
6	0.219	0.219	0.252	0.252	0.282	0.282	0.309	0.309	0.334	0.334	0.357	0.357
5	0.219	0.219	0.252	0.252	0.282	0.282	0.309	0.309	0.334	0.334	0.357	0.357
4	0.219	0.219	0.252	0.252	0.282	0.282	0.309	0.309	0.334	0.334	0.357	0.357
3	0.219	0.219	0.252	0.252	0.282	0.282	0.309	0.309	0.334	0.334	0.357	0.357
2	0.219	0.219	0.252	0.252	0.282	0.282	0.309	0.309	0.334	0.334	0.357	0.357
1	0.219	0.219	0.252	0.252	0.282	0.282	0.309	0.309	0.334	0.334	0.357	0.357

References

[1] Bruyneel M, Fleury C. Composite structures optimization using sequential convex programming. Adv Eng Softw 2002;33:697–711.

[2] Leiva JP, Ghosh DK, Rastogi N. A new approach in stacking sequence optimization of composite laminates using GENESIS structural analysis and optimization software. In: Proceedings of the 9th AIAA/ISSMO Symposium on Multidisciplinary Analysis and Optimization, Atlanta, US-GA; September 4–6, 2002.

[3] Erdal O, Sonmez FO. Optimum design of composite laminates for maximum buckling load capacity using simulated annealing. Compos Struct 2005;71:45–52.

[4] Farshi B, Rabiei R. Optimum design of composite laminates for frequency constraints. Compos Struct 2007;81:587–97.

[5] Rodrigues H, Guedes JM, Bendsøe MP. Hierarchical optimization of material and structure. Struct Multidiscipl Optimiz 2002;24:1–10.

[6] Bendsøe MP, Sigmund O. Topology optimization – theory, methods and applications. 2nd ed. Berlin: Springer; 2004.

[7] Guedes JM, Kikuchi N. Preprocessing and postprocessing for materials based on the homogenization method with adaptive finite element methods. Comput Methods Appl Mech Eng 1990;83:143–98.

[8] Coelho PG, Fernandes PR, Guedes JM, Rodrigues HC. A hierarchical model for concurrent material and topology optimization of three-dimensional structures. Struct Multidiscipl Optimiz 2008;35:107–15.

[9] Coelho PG, Fernandes PR, Rodrigues HC. Multiscale modeling of bone tissue with surface and permeability control. J Biomech 2011;44:321–9.

[10] Yan J, Cheng G, Liu L, Liu S. Concurrent material and structural optimization of hollow plate with truss-like material. Struct Multidiscipl Optimiz 2008;35:153–63.

[11] Andersen CS. Multiscale topology optimization of solid and fluid structures. Ph.D. thesis. Lyngby (Denmark): Technical University of Denmark; 2011.

[12] Nakshatrala PB, Tortorelli DA, Nakshatrala KB. Nonlinear structural design using multiscale topology optimization. Part I: static formulation. Comput Methods Appl Mech Eng 2013;261–262:167–76.

[13] Coelho PG, Guedes JM, Rodrigues HC. Hierarchical topology optimization applied to layered composite structures. In: Proceedings of the 9th World Congress on Structural and Multidisciplinary Optimization, Shizuoka, Japan; June 13–17, 2011.

[14] Reddy JN. Mechanics of laminated composite plates: theory and analysis. Boca Raton: CRC Press; 1997.

[15] Fang K-T, Li R, Sudjianto A. Design and modeling for computer experiments. Boca Raton: Chapman & Hall/CRC Press; 2006.

[16] Lauridsen S, Vitali R, van Keulen F, Haftka RT, Madsen JI. Response surface approximation using gradient information. In: Proceedings of the 4th World Congress on Structural and Multidisciplinary Optimization, Dalian, China; 4–8 June, 2002.

[17] Lund E, Stegmann J. On structural optimization of composite shell structures using a discrete constitutive parametrization. Wind Energy 2005;8:109–24.

[18] Schmidt LA, Miura H. Approximation concepts for efficient structural synthesis. Contractor report CR 2552, NASA; 1976.

[19] Barthelemy JFM, Haftka RT. Approximation concepts for optimum structural design – a review. Struct Optimiz 1993;5:129–44.

[20] Candido GM, Rezende MC, de Almeida SFM. Hygrothermal effects on the tensile strength of carbon/epoxy laminates with molded edges. Mater Res 2000;3:11–7.

[21] Saruyama EH, Okuda IA. Noncircular cross-section carbon fiber, process for producing the same and composite of the carbon fiber with resin. US Patent 5.227.237; 10/1993.

[22] Chung D. Carbon fiber composites. Newton: Butterworth-Heinemann; 1994.

[23] Deng S, Ye L, Mai Y-W. Influence of the fibre cross-section aspect ratio on mechanical properties of glass fibre/epoxy composites – I. Tensile and flexure behaviour. Compos Sci Technol 1999;59:1331–9.

[24] Bond I, Hucker M, Weaver P, Bleay S, Haq S. Mechanical behaviour of circular and triangular glass fibres and their composites. Compos Sci Technol 2002;62:1051–61.

[25] Lee C-Y, Yu W. Homogenization and dimensional reduction of composite plates with in-plane heterogeneity. Int J Solids Struct 2011;48:1474–84.

[26] Xia Z, Zhang Y, Ellyin F. A unified periodical boundary conditions for representative volume elements of composites and applications. Int J Solids Struct 2003;40:1907–21.
[27] Simpson TW, Booker AJ, Ghosh D, Giunta AA, Koch PN, Yang R-J. Approximation methods in multidisciplinary analysis and optimization: a panel discussion. In: Proceedings of the 9th AIAA/ISSMO Symposium on Multidisciplinary Analysis and Optimization, Atlanta, US-GA; September 2–4, 2002.
[28] Etman LFP. Some global and mid-range approximation concepts for optimum structural design. Master's thesis. Eidhoven (The Netherlands): Eidhoven University of Technology; 1992.
[29] Bucher C. Computational analysis of randomness in structural mechanics. Structures and infrastructures, vol. 3. Leiden: Taylor and Francis CRC Press; 2009.
[30] Beachkofski BK, Grandhi RV. Improved distributed hypercube sampling. In: Proceedings of the 43rd AIAA/ASME/ASCE/AHS/ASC Structures, Structural Dynamics and Materials Conference, AIAA-2002-1274, Denver, US-CO; April 22–25, 2010.
[31] Gano SE, Kim H, Brown DE. Comparison of three surrogate modeling techniques: datascape, kriging and second order regression. In: Proceedings of the 11th AIAA/ISSMO Multidisciplinary Analysis and Optimization Conference, Portsmouth, US-VA; September 6–8, 2006.
[32] Sigmund O, Torquato S. Design of smart composite materials using topology optimization. Smart Mater Struct 1999;8:365–79.
[33] Stegmann J, Lund E. Discrete material optimization of general composite shell structures. Int J Numer Methods Eng 2005;62:2009–27.
[34] Lund E. Buckling topology optimization of laminated multi-material composite shell structures. Compos Struct 2009;91:157–8.
[35] Niu B, Olhoff N, Lund E, Cheng G. Discrete material optimization of vibrating laminated composite plates for minimum sound radiation. Int J Solids Struct 2010;47:2097–114.
[36] Stegmann J. Analysis and optimization of laminated composite structures. Ph.D. thesis. Aalborg (Denmark): Aalborg University; 2004.
[37] Bruyneel M, Deltour D, Duysinx P, Gao T, Scoonjans T, Fleury C. New developments in material parametrization for optimal fiber orientations in composite structures. In: Proceedings of the 2nd International Conference on Engineering Optimization, Lisbon, Portugal; September 6–9, 2010.
[38] Bruyneel M. SFP – a new parameterization based on shape functions for optimal material selection: application to conventional composite plies. Struct Multidiscipl Optimiz 2011;43:17–27.
[39] Reddy JN. An introduction to the finite element method. 2nd ed. New York: McGraw-Hill; 1996.
[40] Haftka RT, Gurdal Z. Elements of structural optimization. 3rd ed. Dordrecht: Kluwer; 1992.
[41] Luenberger DG. Linear and nonlinear programming. 2nd ed. Norwell: Kluwer; 2003.
[42] DOT (Design Optimization Tools) Bruchure, Vanderplaats R.&D. Inc., Colorado Springs, US-CO; 2008. <www.vrand.com>.
[43] Vanderplaats GN. Numerical optimization techniques for engineering design. New York: McGraw-Hill; 1984.
[44] Ferreira RTL, Hernandes JA. New approximations for sequential optimization with discrete material interpolations. In: Proceedings of the 10th World Congress on Structural and Multidisciplinary Optimization, Orlando, US-FL; May 19–24, 2013. <http://www2.mae.ufl.edu/mdo/Papers/5076.pdf>.
[45] Pedersen P. On optimal orientation of orthotropic materials. Struct Optimiz 1989;1:101–6.
[46] Lucena Neto E. Fundamentals of elasticity and plasticity. Instituto Tecnológico de Aeronáutica, São José dos Campos, SP, Brazil; 2006 [Class Notes].
[47] Maligno AR. Finite element investigations on the microstructure of composite materials. Ph.D. thesis. Nottingham (United Kingdom): The University of Nottingham; 2007.
[48] Vaughan TJ, McCarthy CT. Micromechanical modelling of the transverse damage behaviour in fibre reinforced composites. Compos Sci Technol 2011;71:388–96.
[49] Yang L, Yan Y, Liu Y, Ran Z. Microscopic failure mechanisms of fiber-reinforced polymer composites under transverse tension and compression. Compos Sci Technol 2012;72:1818–25.